Laser Optics for a $\gamma\ \gamma$ Collider*

D.E. Klem, L. Seppala
Lawrence Livermore National Laboratory, Livermore, CA 94551 USA

ABSTRACT

The constraints on an optical system to convert the electron beams to γ-ray beams for a $\gamma\ \gamma$ collider are considered. We show that the range of possible designs is limited by the requirement of near head-on collisions and present a design which achieves two passes of the laser pulse with arbitrary control of the polarization. For certain polarization combinations, four passes appear possible.

I. INTRODUCTION

The basic idea of a $\gamma\ \gamma$ collider [1] has been introduced in the paper by Takahashi [2] in these proceedings. In this paper we consider the realities of bringing the laser to the conversion point (CP) inside a detector. Because of the desire for a detector with 4π coverage, access to this region is limited. The difficult issue of backgrounds from the intense e^- beams further complicates the situation.

Table I: Electron beam parameters assumed at the CP.

Parameter	Value
crossing angle	$\pm$15 mrad
disrupted beam size	$\pm$10 mrad
μ-rep. rate	1.4 nsec
macro-rep. rate	180 hz
# of μ-pulse per macro-pulse	90
horizontal beam size	σ_x^* = 71.5 nm
vertical beam size	σ_y^* = 9.04 nm
μ-bunch length	σ_z = 100 μm
electron energy	250 GeV
electrons / bunch	$6.5 \cdot 10^9$

The parameters assumed for the electron beams in this study are given in Table I. They follow the NLC design parameters [3]. The laser beam parameters required at the conversion point (CP) are given in Table II. The single pulse characteristics required at the CP have been discussed previously [3]. The pulse length must match the length of the electron bunch. The intensity must be low enough to avoid non-linear effects in the conversion. The integrated intensity seen by the electron bunch must be sufficient to convert about two thirds of the incident electrons (a fluence greater than this generates an excessive number of low energy backscattered photons). A detailed optimization has been performed [3]. While the energy of 1 J which results from the optimization is below the single pulse energy which has been available for a substantial length of time, the very high repetition rate and its associated very high average power at the conversion point (16.2 kW) have not been demonstrated to date.

Table II: Laser parameters required at each CP.

Parameter	Value
peak intensity	$10^{18} W/cm^2$
energy / μ-pulse	1 J
wavelength	λ = 1.05 μm
pulse length	τ = 1.8 psec
μ-rep. rate	1.4 nsec
macro-rep. rate	180 hz
# of μ-pulses	90
focusing	f/10 Gaussian equivalent
Rayleigh range	z_R = 100 μm
average power	16 kW each side
polarization	left, right, horizontal, vertical

II. CONSTRAINTS ON THE LASER FOCUSING OPTICS

Given that the cost of the laser required will be a major component of the total cost of a second IR at the NLC and given that the cost of such a laser is likely to proportinal to its power, it is clear that considerable care must be taken to achieve the highest efficiency in the transport and conversion processes.

A. B-integral effects

Because of the extremely high peak intensities involved even in the *unfocused* pulses required here, the use of transmissive optics such as lenses, polarizers, and Pockels cells is generally very limited and propagation in air is not possible over long distances. This occurs because of a non-linearity in the index of refraction for the materials involved and is expressed in terms of the B-integral [4]:

$$B = \frac{2\pi}{\lambda} \int_0^L n_{2I}(z) I(z) dz \qquad (1)$$

where n_{2I} expresses the degree of non-linearity, and the integration is along the direction of propagation. Values of B greater than about three generally will lead to degradation of the focusability of the pulse. Fused silica has an $n_{2I} = 2.8 \cdot 10^{-16} cm^2/W$. This results in a limit on the order of a few centimeters of fused silica for the beam sizes considered here.

*This work was performed under the auspices of the U.S. Department of Energy under contract No. W-7405-Eng-48.

This effect pushes the design toward one which uses almost all reflective optics [5] with the limited B-integral "budget" allocated to vacuum windows, waveplates, and possibly polarizers. Note that this limitation becomes particularly important for any multipass scheme as the effect integrates with each pass.

B. Laser Damage to Optics

While the combination of extremely intense pulses and a very high average power represents an unexplored area for this issue, the known damage thresholds do not suggest the existence of a problem. Laser damage to dielectric coatings such as would be used here is understood in terms of energy transfer from the fields of the laser pulse to electrons in the dielectric, followed by transfer of the electron energy to the lattice. The measured dependence of damage thresholds on pulse length is consistent with this picture [6]. We can consider three time scales in the present situation:

- **short pulse** (psec) limit: 0.7-2 J/cm^2 at 1.8 psec [7].
- **long pulse** (nsec) limit: 100-200 J/cm^2 at 126 nsec [7].
- **average power** limit: 3-5 kW/cm^2 routine at AVLIS [8].

where these represent the effect of a single laser pulse, the macro-pulse, and the average respectively. For the situation considered here, the actual minimum mirror size comes from the average beam power with the short and long pulse limits providing constraints that are about a factor of three to four weaker.

C. Laser Focusing

The optimization referred to above assumes a Gaussian beam profile. In practice a flat top beam of similar energy is more economical to produce. Such a beam focuses to an Airy pattern in the focal plane as opposed to a Gaussian. A comparison of the relevant parameters is given in Table III. The main point is that a similar dependence of intensity on position near best focus is obtained when $f_{\#flattop} = 0.7 \cdot f_{\#Gaussian}$.

Table III: Focusing of flattop and Gaussian beams. I is the intensity. The "area" here is defined as the total power divided by the *peak* intensity I_0.

	Flattop	Gaussian
$I(r, z=0) =$	$I_0 \left[\frac{2J_1(r/s)}{r/s}\right]^2$	$I_0 \exp\left(-2\frac{r^2}{w_o^2(1+z^2/z_R^2)}\right)$
	$s = \frac{f_\# \lambda}{\pi}$	$w_0 = \frac{2 f_\# \lambda}{\pi}$
$I(r=0, z) =$	$I_0 \left[\frac{\sin(z/z_0)}{z/z_0}\right]^2$	$I_0 \left[1 + \left(\frac{z}{z_R}\right)^2\right]^{-1}$
	$z_0 = \frac{8}{\pi} f_\#^2 \lambda$	$z_R = \frac{4}{\pi} f_\#^2 \lambda$
"Area"=	$\frac{f_\#^2 \lambda^2}{\pi} = \pi s^2$	$\frac{2 f_\#^2 \lambda^2}{\pi} = \frac{\pi w_0^2}{2}$

D. Polarization

The control of the polarization of the final γ beams is an important tool for accessing the full range of physics available to a $\gamma\ \gamma$ collider. The polarization of the Compton scattered gamma is a function of the polarization of both the initial electron and the initial laser photon [9]. Since the polarization product $(2\lambda_e P_c)$ affects both the polarization of the final gamma as well as its distribution in energy and angle, it is necessary to match the polarization of the laser and the electron beam so that the backscattered beam peaks at its maximum energy. This effect is shown in Fig. 1. The desired case occurs when $2\lambda_e P_c = -1$.

For the pulse compressed laser systems that will be used for a $\gamma\ \gamma$ collider, it is likely that the output of the laser system proper will be limited to linear polarization in a fixed direction due to the behavior of the gratings in the compressor. This polarization can then be manipulated with a $\frac{1}{4}$-wave plate [10]. Wave plates exploit the anisotropic behavior of certain crystals. The directionality of the crystal defines three principal axes, each with a separate dielectric constant. A wave plate consists of a thin piece of an appropriate crystal with one principal axis oriented along the direction of propagation. The two remaining axes have different propagation velocities due to their different ϵ's. A quarter wave plate ($\lambda/4$ plate) is obtained if the thickness of the plate is choosen so that the total delay equals one quarter of a wavelength [11]. The orientation of the crystal axes with respect to an incident linearly polarized beam determines the details of conversion between various polarization states. By orienting the crystal so that the incident laser polarization is 45° from both axes, a circularly polarized beam is produced as shown in Fig. 2. Alternately, an incident circularly polarized beam produces a linearly polarized beam whose polarization is determined by the orientation of the crystal.

From the preceding it is clear that changing the polarization of the laser pulse at the CP is essentially a *mechanical* operation since it involves moving the waveplate. As such, it will probably take on the order of seconds. This would limit the time between

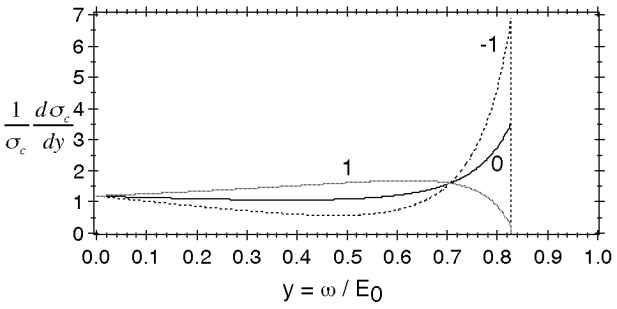

Figure 1: The energy distribution of the backscattered laser photons for three different values of the polarization product. The desired case of the distrubution peaking at the maximum energy occurs for $2\lambda_e P_c = -1$.

polarization changes to some minutes, which is still probably short enought to adequately average over systematic changes in the behavior of the detector or beams.

E. Crossing Angles and Aspect Ratios

Probably the most significant constraint on any realistic scheme for converting the electron beam comes from the requirement that the electron bunch and the laser pulse pass through each other head-on such that every electron "sees" every laser photon [12]. The luminosity from two bunches crossing each other at an angle θ relative to head on is given by [13]:

$$\frac{L(\theta)}{L(\theta_0)} = \left[1 + (\theta/\theta_0)^2\right]^{-\frac{1}{2}} \quad ; \quad \theta_0 = \left[\frac{\sigma_{x1}^2 + \sigma_{x2}^2}{\sigma_{z1}^2 + \sigma_{z2}^2}\right]^{\frac{1}{2}}. \quad (2)$$

and the σ_x's and the σ_z's are the transverse and longitudinal beam sizes respectively. Since it is clear inour case that the dominant terms come from the size of the laser beam, this expression can be reduced to:

$$\frac{L(\theta)}{L(\theta_0)} = \left[1 + \theta^2 \frac{\sigma_z^2}{\sigma_t^2}\right]^{-\frac{1}{2}}. \quad (3)$$

The crossing angle must remain small compared to the aspect ratio σ_t/σ_z of the laser pulse if there is not to be a significant degradation of the conversion efficiency. This angle can be compared to the angles which characterize the focusing of the laser beam. From Table III the angle between the central ray and a peripheral ray is $\frac{1}{2f_\#}$. The aspect ratio is given by $\frac{2z_R}{w_0} = 4f_\#$. So if the electron beam is tangential to the cone of the focusing laser beam, then the conversion would only be 45% of the head-on case. From this consideration it is clear that a solution which has the electron beams passing through the laser focusing optic will result in a much lower requirement on average laser power.

Since a hole to allow the beam to pass through the mirror occurs near the worst spot for a Gaussian beam profile, it is another reason to prefer a flattop. The effect of such a hole on the focusing is to "loose the energy twice." Once for the obvious reason, and a second time because diffraction will put an equal amount of energy into a large focal spot corresponding to the size of the hole in the mirror.

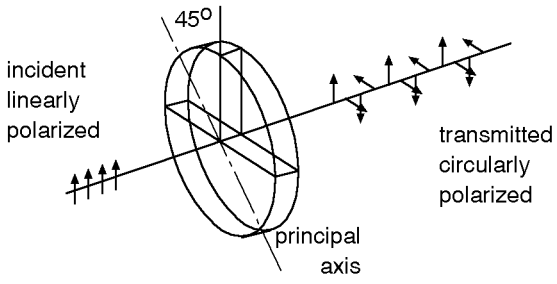

Figure 2: Effect of a waveplate on a linearly polarized beam.

F. Spent Beams and the Hole in the Mirror

While the incident electron beams are small on most of the scales relevant to a $\gamma\ \gamma$ collider, the disruption of the beams which occurs during the conversion gives them a significant angular spread. These spent beams must have a clear path out of the detector in order to avoid the creation of unacceptable backgrounds. Similarly, the optical beams, with their average powers of 16kW each, must also be transported away from the conversion points. These considerations combined with the constraint that the optical axis must be nearly coincident with the axis of the electron beam lead to the situation summarized in Fig. 3. In this figure the two large circles show the angular region necessarily occupied by the two laser beams (one on its way toward a CP, the other a "used" beam leaving the other CP). The two small circles show the region around a spent electron beam (only one or the other would be needed on a single side).

This multiple overlap implies that the final focusing optic for the laser will also be required to at least transport the "spent" beam from the other side out of the detector. If the two conversion points were coincident, then the overlap in position and angle would be exact and it would not be possible to separate the two optical paths using only reflective optics. The small transverse offset between the two conversion points will eventually cause the beams to walk off from each other. Alternately, the small mismatch in focal lengths will cause one beam to eventually diverge.

In addition, it is necessary to leave a clear path through the detector for the synchrotron radiation generated up stream of the detector in bending and focusing magnets [14]. Since this radiation is expected to be essentially parallel to the electron beams, this requirement is most easily met if the final mirror is located a substantial distance from the detector.

Lastly, the forward region being considered here has been commonly used to determine the luminosity by measuring the rate of a small momentum transfer process with a known calculable cross section (such as Bhabha scattering in the case of

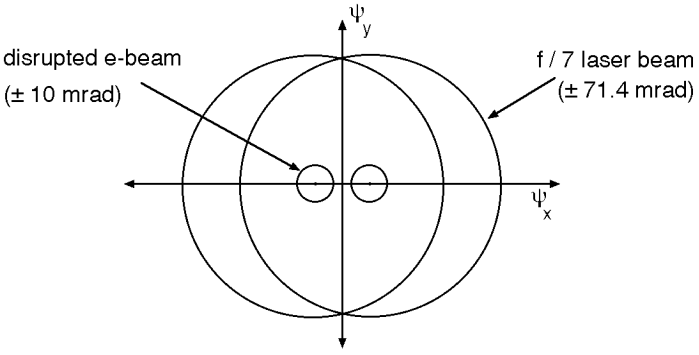

Figure 3: Occupancy of angular regions around the beam. The desired focusing (f/7 flattop) implies a beam that occupies a region large compared to both the disrupted beam size and the separation between the incoming and outgoing beams.

e^+e^-). Since the thickness of this optic will be rougtly $\frac{1}{6}$ of its diameter, there is a clear compromise to be made with respect to the location of the final focusing mirror. The further back this mirror is placed, the greater its thickness and the more likely it is to degrade this measurement. The closer in, the greater the effect of the hole.

G. Multi-passing

Because of the tremendous disparity in the number of particles in the laser pulse as opposed to the electron bunch ($6.5 \cdot 10^9$ electrons verses $7 \cdot 10^{18}$ photons), the laser pulse is not in any sense consumed in the interaction with the electron beam. It would therefore be very useful if the pulse could be reflected back and used again to convert subsequent pulses. Any such scheme clearly runs into serious difficulties given the overlap of the optical paths shown in Fig. 3.

Overall path lengths also pose a constraint on any multipass scheme. The entire macro-bunch occupies a time internal of only 126 nsec or a distance of only 37.8 m. Any beam path associated with a multipass scheme must be less than half of this in order to get at least two passes. This means, for instance, that any scheme in which the beam must pass around the outside of a LEP scale HEP detector is unlikely to get more than two passes. It also means that schemes which retroreflect the pulse generally will do better than ring schemes because they do not waste the time to get back to the other side of the detector. Note that the walk off discussed in a previous section will only occur over distances which are not useful for multipass schemes due to the propagation delays being at least of order of the total length of the macro bunch.

While controlling the polarization in a single pass scheme is clearly trivial, multiple pass schemes present additional complications because we no longer have the possibility of an independant waveplate in every path.

III. LAYOUT

The complete optics design located inside a hypothetical cylinderical detector is shown in Fig. 4 and in close-up in Fig. 5. The use of a compromise optical axis and a double pass scheme is clearly suggested by Fig. 3 and has been implemented here. The beam enters from the right in Fig. 4 and converts the electron beam entering from the left. After passing through the system of focusing mirrors on the left it is reflected back through the same system to focus 1 cm past the previous focus to convert the opposite electron beam [15]. The cylindrical objects located inside the masking on either side are "place holders" for the final quadrapoles.

The penalty for being slightly off axis is a factor of 0.86 (from Eq. 3). The savings in laser energy from the two passes is diluted by the time delay between the two the CP's which requires an additional 16 pulses. The net effect is to reduce the required power by a factor of 0.68.

Detector and optics parameters are summarized in Table IV. In this configuration the vertex chamber is essentially unobstructed, only having to avoid the masks and the focused laser beams. This also provides the maximum access for a sweeping magnet [3] to separate the spent electron beams in order to reduce the e^-e^- and γe^- luminosities.

Table IV: Parameters for the detector and laser at input to optics on detector.

Parameter	Value
masking	135-185 mrad
distance to 1^{st} quadrapole	>1.6 m
distance to 1^{st} mirror	1.5 m
inner radius of vertex chamber	2 cm
solid angle for vertex chamber	0.97 (inner radius)
clear aperture around beam	3 cm
$f_{\#}$ of focusing optic	8.76 / 5.58
beam profile	7.58 cm x 4.85 cm flattop
energy / pulse	1.33 J
# of μ-bunches	106
average power	25.4 kW total

A. Focusing Optics

The design of the four mirror telescope used to focus the laser beam at the CP is shown schematically in Fig. 6. The sizes and locations of the mirrors as well as thier curvatures are given in Table V. Because these optics place a limit of sorts on the angular acceptance of the detector, it is desirable to contain the entire system inside as small a cone as is possible. Toward this end, a slighly elliptical beam with an aspect ratio of 1.56 is used. This allows the entire system to be located inside a cone of 135 mrad. With simple spherical mirrors this design obtains a Strehl ratio [16] of 0.90. With one slightly aspheric surface this can be

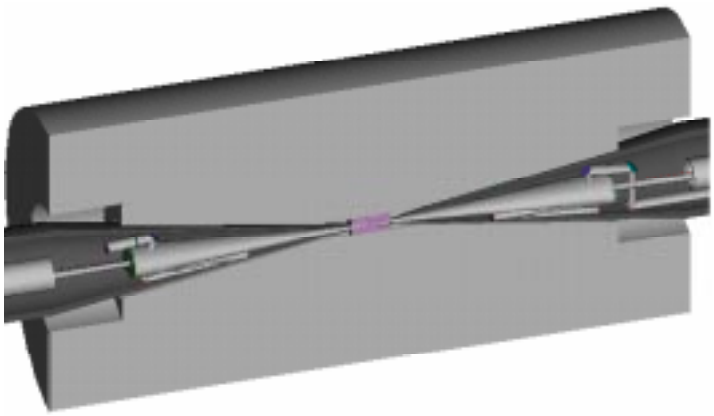

Figure 4: The layout of the laser optics in a hypothetical cylinderical detector. The laser beam enters from the right. A single $\frac{\lambda}{4}$ plate is located between the last turning mirror and the retromirror on the far left. The cylinderical objects located inside the masking on either side are place holders for the last quadrapole.

increased to 0.99. Hence the actual Strehl ratio achieved will not be limited by the optics design, and this is achieved without resorting to such things as large off-axis paraboloids. The total path length through this system is 3.18 m which corresponds to a time delay of 10.6 nsec or about 7.5 micro-bunch crossings. The hole in the mirror consists of a pair of 1.5 cm radius holes (corresponding to the $\pm$ 10 mrad spent e^- beam) plus the area between them. This represents 3.8% of the total beam area. All of the optics in this design have sufficient area to be below the damage thresholds listed in Section II.B.

Table V: Parameters of the optical design (in mm).

what	beam size		location		mirror	distance to
	x	y	x	y	radius	next mirror
f_p	0	0	0	-1500		1500
M1	171	269	0	0	1207	730
M2	47	75	-76	-726	570	650
M3	45	72	-144	-80	6600	300
M4	49	73	150	-141	9227	

B. Polarization

A scheme of polarization control is shown in Fig. 7(a). The polarizations of the beam at various locations for various configurations of the waveplates is given in Table VI. This scheme shows that it remains possible to have full control of the laser polarization at both CP's even though the beam retraces its path for the second pass.

C. Luminosity Measurements

The last focusing mirror (M1 in Fig. 6) will have a thickness of about 4.5 cm and is likely to be made from fused silica. This correspondes to 0.37 radiation lengths in the region $\cos\theta >$ 0.9984 to 0.9960 depending on azimuth.

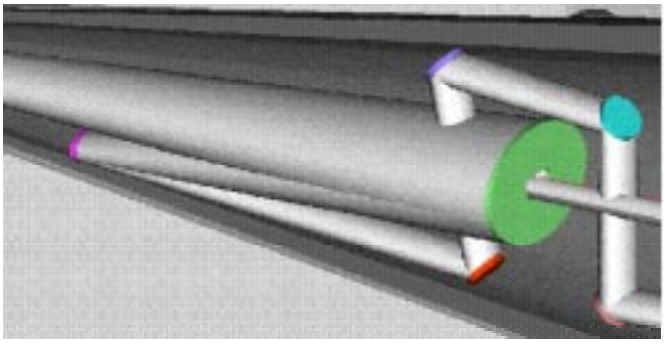

Figure 5: Close up view of the laser optics on one side. Final focusing mirror has hole for electron beams. The optics on the opposite side are identical except for the presence of a retromirror in place of the last turning (flat) mirror shown here.

Table VI: Polarization states obtained in the two pass scheme shown in Fig. 7. The first two columns refer to the presence or absense of the wave plate at the two positions indicated. The last six columns give the polarization at the six locations indicated in the figure. The two bold face columns are at the conversion points.

pol-A	pol-B	1	2	3	4	5	6
out	out	hor.	**hor.**	hor.	hor.	**hor.**	hor.
in	out	hor.	**right**	right	left	**left**	vert.
in	in	hor.	**right**	vert.	vert.	**right**	hor.
out	in	hor.	**hor.**	right	left	**vert.**	vert.

Several additional mirrors are located in the region between the M1 mirror and the mask. Similar scaling applies to their thicknesses, so they will contribute of order 0.1 radiation lengths of material. Since they occupy only a limited fraction of the azimuth, this is presumably less of a problem. Support structures will clearly add to these numbers.

D. More than two passes

A scheme for obtaining a total of four passes is shown in Fig. 7(b). This scheme will only work for the cases on lines two and four of Table VI where the polarization gets a net 90° rotation in passing through the system in Fig 7(a). In this case it can pass through the polarizer shown and be reflected back through the system for another pass. We note that even an ideal "switch" at this point can only obtain approximately three passes because of the 30 nsec transit time through the focusing optics.

IV. SUMMARY AND CONCLUSIONS

We have shown a scheme for integrating the conversion of e^- beams into γ beams inside the constraints of a conventional HEP detector. No impact is made on the location of the vertex chamber and the masking need only extend to 185 mrad. A clear apature around the beam with a diameter of 3 cm can be maintained with only a 7.6% increase in the required laser power. This is likely to be critical in minimizing backgrounds in the detector.

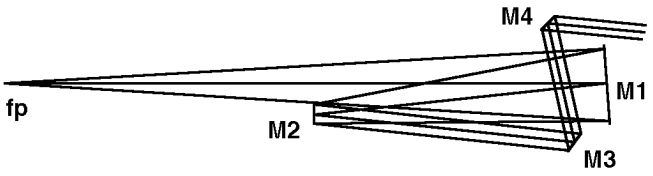

Figure 6: A schematic view of the four mirror telescope to focus the laser. The parameters of the design are given in table V. The slighly elliptical beam has its narrow dimension in the plane of the paper.

While many issues remain, no show stoppers have been found so far. Some of the issues to still be examined include: radiation damage of optics affecting the laser damage threshold, the heat load due to mirror leakage, background calculations, and detailed calculations on luminosity measurements.

The authors acknowledge useful conversions with Kwang-Je Kim, Ming Xie, Valery Telnov, and Mike Perry.

V. REFERENCES

[1] Ginzburg et al., JETP Lett 34 (1982) 491.

[2] See the article by T. Takahashi et al. in these proceedings.

[3] *Zeroth-order Design Report for the Next Linear Collider* SLAC-474 (1996).

[4] W. Koechner, *Solid State Laser Engineering* (Springer-Verlag, New York, 1988), chapters 4,11.

[5] In this context this means multilayer dielectric coatings.

[6] B.C. Stuart et al., PRL 74 (1995) 2248.

[7] B.C. Stuart private communication.

[8] Ed English private communication.

[9] Valery Telnov, NIM A **355** 3 (1995).

[10] M. Born and E. Wolf, *Principles of Optics* (Pergamon, New York, 1980), chap. 14.

[11] In practice $\lambda/4$ plates are usually made from two plates: one $(n+1/4)\lambda$ and a second $(n+1/4)\lambda - n\lambda$ so that the plates have sufficient mechanical strength.

[12] The crab crossing scheme overcomes this difficulty by rotating the bunches so their axes are both oriented along an "average" axis. Because we require crabbing of the final gamma beams (and therefore crabbing of the electron beams), it is not possible to crab the electron-laser crossing in an exact manner. This appears to exclude crabbing in the present context, even if a scheme for generating a "crabbed" laser pulse could be found.

[13] M. Xie et al., NIM A **355** 163 (1995).

[14] SLD experience suggests 2 cm in radius. (Stan Hertzbach private communication.) The issue is a trade off between efficient use of the laser energy and backgrounds.

[15] This implies a slight "tweak" to the optics on the left side. If we allow the retromirror to be slightly spherical, then we can control both the position and the $f_{\#}$ of the reflected beam.

[16] W. Smith, *Modern Optical Engineering* (McGraw-Hill, New York, 1990), p. 336.

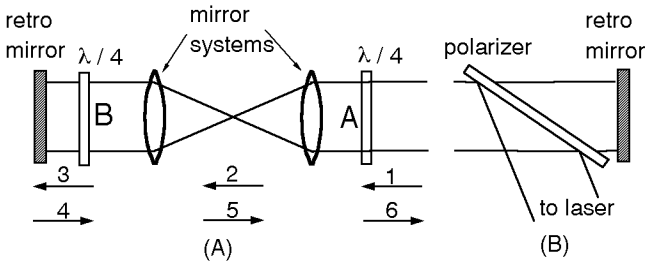

Figure 7: The location of $\frac{\lambda}{4}$ plates in a two pass scheme is shown in part (a). The polarization states obtained are listed in Table VI. The lenses shown represent the focusing system shown in Fig. 6. Part (b) shows the scheme for obtaining four passes discussed in Section III.D.